Biophysical Journal
Article

Biophysical Society

Signal Destruction Tunes the Zone of Activation in Spatially Distributed Signaling Networks

Kalinga Pavan Silva,[1] Prithiviraj Chellamuthu,[1,2] and James Q. Boedicker[1,2,*]
[1]Department of Physics and [2]Department of Biological Sciences, University of Southern California, Los Angeles, California

ABSTRACT Diverse microbial communities coordinate group behaviors through signal exchange, such as the exchange of acyl-homoserine lactones (AHLs) by Gram-negative bacteria. Cellular communication is prone to interference by neighboring microbes. One mechanism of interference is signal destruction through the production of an enzyme that cleaves the signaling molecule. Here we examine the ability of one such interference enzyme, AiiA, to modulate signal propagation in a spatially distributed system of bacteria. We have developed an experimental assay to measure signal transduction and implement a theoretical model of signaling dynamics to predict how the system responds to interference. We show that titration of an interfering strain into a signaling network tunes the spatial range of activation over the centimeter length scale, quantifying the robustness of the signaling network to signal destruction and demonstrating the ability to program systems-level responses of spatially heterogeneous cellular networks.

INTRODUCTION

Microbes use small-molecule signals to coordinate group behaviors. For example, many Gram-negative bacteria exchange acyl-homoserine lactones (AHLs) to regulate quorum sensing and related emergent behaviors such as biofilm formation, collective motility, bioluminescence, and virulence (1–4). Activation of quorum sensing involves the production of a signal by a synthase, for example, LuxI, used here, which was isolated from *Aliivibrio fischeri*. The signals exit the cell either by passive diffusion through the membrane or by active transport (5), and they can be detected in neighboring cells by specific receptors, here the receptor LuxR. Binding of the signal to the receptor leads to global changes in gene expression. The signals enable bacteria to relay information about their physical, chemical, and biological environment (6–10). Communities that coordinate behavior through such mechanisms often have a fitness advantage (11,12). Not surprisingly, other bacteria have evolved mechanisms to interfere with the signaling process.

Bacteria exhibit various signal interference mechanisms (13,14); collectively, these mechanisms that interfere with bacterial cell communication have been termed quorum quenching (13,15,16). The two main mechanisms of quorum quenching found in natural communities are signal crosstalk and signal destruction. Signal crosstalk between related signals can result in competitive binding to the receptors (13,17,18), and some bacteria produce compounds whose only known function is receptor antagonism (13,15,16). Signal destruction often involves the production of an enzyme that chemically modifies or cleaves signaling molecules. The influence of signal destruction on signaling propagation through space has not been systematically explored.

Here, we develop an experimental assay to quantify multispecies pattern formation. The assay enables direct measurement of the robustness of signal exchange to the introduction of a variable amount of a signal-degrading strain. Since the initial work by Basu et al. (19), demonstrating the ability to program pattern formation through signal exchange, several studies have examined many aspects of bacterial pattern formation. Experimental works have examined scale-invariant patterns (20), the impact of signal removal on long-distance signaling (21), tuning the concentration dependence of the bacterial response to signal (22), multispecies pattern formation that was programmable and robust to environmental perturbations (23), the control of pattern formation coupled to motility (24), and the ability of signal degradation to impact wild-type behaviors such as biofilm formation and swarming (25). Theoretical advances have also deepened our understanding of the sensitivity of patterns to model parameters (26). Here, we build upon these previous studies to

Submitted August 30, 2016, and accepted for publication January 10, 2017.
*Correspondence: boedicke@usc.edu
Editor: Reka Albert.
http://dx.doi.org/10.1016/j.bpj.2017.01.010

determine what level of interference can be tolerated by a microbial network exchanging AHLs, and we predict and experimentally validate changes in the signaling patterns in the presence of interference.

Interference by signal-destroying enzymes is a potential route by which to control bacterial community function in industrial and biomedical applications. For instance, signal destruction can be used to limit cell-cell communication in microbes, which has been directly linked to pathogenicity (13,15,16). The ability to precisely program and control emergent behaviors of microbial networks through molecular-level manipulation requires a thorough, quantitative understanding of signal exchange and interference in mixed communities. Although previous studies (13,15,16,19) have identified many natural systems with signal interference, no quantitative measurements have been taken to understand the robustness of signal exchange in spatially heterogeneous systems in the presence of interference. Here, we developed an experimental assay to examine the influence of a signal-destroying enzyme, the lactonase AiiA, on the spatiotemporal dynamics of signal exchange in a multistrain synthetic signaling network. The assay measures the robustness of signaling to interference. We find that AHL signaling in the presence of an interference strain producing the enzyme AiiA results in a limited zone of activation. Using a theoretical model, we show that the size of this zone is tunable by adjusting the number of interfering cells and signal-producing cells. These results demonstrate that signal interference limits the spatial range of activation in the vicinity of a signal-producing colony and can be implemented to predictably program the response of multistrain bacterial communities.

MATERIALS AND METHODS

Bacterial strains and plasmid

The sender strain is *Escherichia coli* (*NEB 5-alpha*) with the plasmid ptD103luxI sfGFP(Kn) (Fig. S1) from (27). This strain produces the signal N-(3-oxohexanoyl)-HSL and the cognate receptor LuxR. The GFP reporter gene activates in response to quorum-sensing activation. The interfering strain consists of an *E. coli* host harboring the plasmid ptD103aiiA(Cm) (see Fig. S2 *A* and (27)).

The receiver strain is *E. coli* (*NEB 5-alpha*) with the plasmid pTD103LuxR RFP, shown in Fig. S3. To construct the receiver strain, the plasmid pTD103luxI sfGFP(Kn) was mutagenized by inserting *mCherry* in the position of *sfGFP*, using a Gibson assembly kit (New England Biolabs). The receiver strain plasmid expresses *mCherry* fluorescent protein in response to quorum-sensing activation.

Culturing conditions

Bacterial strains were taken from frozen stocks and grown in a 14 mL Falcon tube with 5 mL of lysogeny broth (LB) with appropriate antibiotics for plasmid maintenance. Cultures were grown in a shaker at 220 rpm and 37°C. After 16 h of growth, the culture in the late log-phase was taken out and 1 mL of the inoculum was transferred into a micro-centrifuge tube. The tube was centrifuged at 15,000 rpm for 1 min and the supernatant was discarded. The cells were then resuspended by vortexing in LB without antibiotics. Late log-phase cultures were used such that quorum sensing of the sender strain was activated before measurement in the plate assay, in which LB agar with 2.5% agar was used. During time-lapse experiments, the cells were imaged at 37°C.

Interference assay

Ten microliters of the receiver strain was mixed with the interference strain in a micro-centrifuge tube. The mixture was loaded onto an LB agar plate by pipetting, and cells were distributed evenly using 4-mm-diameter sterilized glass beads. After 10 min, 1 μL of the sender strain was pipetted to the middle of the plate. The plate was imaged using a fluorescent microscope for time-lapse experiments.

Microscopy measurements

The images were taken using a Nikon eclipse TI fluorescent microscope. Time-lapse experiments were carried out at 37°C using a temperature-controlled chamber. Samples were imaged with green (GFP) and red fluorescent protein (RFP) illumination at a magnification of 20×. RFP images were taken every 15 min for 16 h at 30 different distances from the sender colony, extending in two directions outward from the sender colony. Activation times were calculated at each position. Exposure time at each position was 1 s for RFP and 500 ms for GFP. No significant photobleaching was observed.

Each image taken was saved in .tiff format and analyzed using a custom MATLAB code. A low threshold was applied to the RFP images to identify the location of receiver cells within each image. An upper threshold was used to identify the receivers that had activated quorum sensing. For each time point and position, the fraction of cellular pixels above the quorum-sensing-activation threshold was calculated. If the fraction of activated pixels exceeded 10%, that position was included as part of the activated region.

Growth measurements

To obtain the growth curves, the cells were grown in LB media with appropriate antibiotics, as mentioned above. After 16 h growth, we diluted 5 μL of the cells in 4995 μL of LB. Dilutions of the culture were plated on selective media to measure cell density over time.

To test the growth influences on the receivers and senders when in coculture with the interferers, we diluted 5 μL of the senders (or receivers) with 5 μL of the interferers in 4990 μL of pure LB broth, and the previous procedure was repeated by selecting for the senders and receivers using proper antibiotic plates.

Plate-reader measurements

A Tecan Infinite m200 Pro plate reader was used to measure growth rates and fluorescence in well-mixed conditions. Cells were grown in LB media, as mentioned above. Cells were then diluted 1000-fold in LB media containing antibiotics and cultured for an additional 3 h. After 3 h of growth, 200 μL of these early log-phase cells were loaded into a flat bottom 96-well plate. The plate was inserted into the plate reader set to 37°C and the optical density and fluorescent intensity were measured every 15 min for 15 h. Optical density measurements were carried out at a wavelength of 600 nm. For GFP measurements, a wavelength of 485 nm was used for excitation and a wavelength of 515 nm was used for emission. For mCherry fluorescence measurements, a wavelength of 590 nm was used for excitation and a wavelength of 650 nm was used for emission. In the Supporting Material we introduce a method for analyzing the fluorescence of a single species from a mixed culture.

RESULTS AND DISCUSSION

Quantifying signal exchange in spatially distributed microbial networks

An assay was developed to examine the dynamics of signal exchange in multistrain bacterial communities. The assay is based on previous reports that used solid agar plates to measure the response to the diffusive exchange of signaling molecules (19–22). As shown in Fig. 1 *a*, our system consists of a 2.5% LB plate with a receiver strain evenly distributed on top of the plate. The receiver strain does not produce the signal (AHL); however, it produces the receptor LuxR and increases the expression of a fluorescent reporter gene, mCherry, in response to the AHL signal. A sender strain containing the synthase gene *luxI* produces the AHL signal and is pipetted onto the center of the plate. The sender strain makes the receptor LuxR, and as in the natural quorum-sensing system, the synthase is positively regulated by AHL. The sender strain produces GFP. Control measurements reported in Fig. S4 show that the fluorescence intensity of the receiver strain increases upon coculture with the sender strain. *E. coli* strains contained plasmids based on constructs reported in (27) (see Figs. S1–S3). Similar sender/receiver systems have been developed and investigated in previous work (19,28–38).

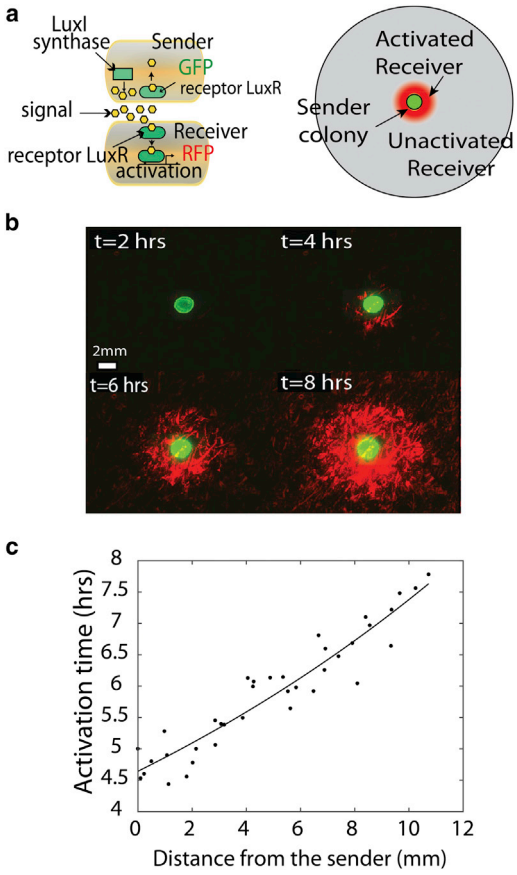

FIGURE 1 (*a*) The two-strain signaling network consists of a sender strain (GFP) producing AHL signal and a receiver strain (mCherry) containing an AHL-regulated fluorescent reporter gene. In the plate assay, the receivers are evenly distributed on an LB-agar plate, and a colony of sender strains is added to the middle of the plate. (*b*) Time-lapse fluorescent imaging captures the activation of the receiver cells as AHL diffuses outward from the sender colony. The green fluorescence shows the location of the sender strain. (*c*) Activation time of the receivers as a function of distance from the sender colony. The data points have been fitted to an exponential curve. To see this figure in color, go online.

Upon adding the sender strain to the center of the plate, the sender strain excretes AHL signal, which diffuses into the lawn of receiver strains to activate expression of a fluorescent reporter gene (mCherry). As shown in Fig. 1 *b*, the receiver cells closest to the sender cells are activated first, and over time, this region of activation expands outward. Fluorescent images, shown in Fig. 1 *b*, represent the stitching together of images from several microscope positions taken at 20× magnification such that activation can be observed at the single-cell level over centimeter length scales. The dynamics of signal exchange in the system can be quantified by measuring the time at which receiver cells activate at a specific distance from the center of the sender cells. We set a threshold pixel intensity to indicate this transition from the basal to the activated rate of fluorescence expression (see Fig. S5). Quorum-sensing activation at a given position is defined as 10% of the pixels belonging to cells being above this threshold. In Fig. S6, we show that the activation dynamics are not strongly dependent on the value of the activation threshold used in the analysis. Fig. 1 *c* shows the dynamics of activation at distances of up to 12 mm from the sender colony, the size of the plate used in the assay.

AiiA inhibits quorum sensing in a synthetic microbial community

To extend the signaling assay to the examination of interference between strains, we first validated the interference capabilities of a strain producing the enzyme AiiA, a lactonase originally isolated from *Bacillus thuringiensis* (13,15,16). A plasmid containing *aiiA*, from (27), was transferred to *E. coli* to create the interference strain and added to the sender-and-receiver community, as depicted in Fig. 2 *a*.

Fig. 2 *b* shows the activation of quorum sensing for the sender strain alone and in coculture with the AiiA interference strain. Here, the fluorescence intensity of the sender strain was measured in a 96-well plate reader under well-mixed conditions. Coculture with the interference strain reduced the level of quorum-sensing activation, indicating that the AiiA producing strain interfered with AHL signal transduction. We did not observe significant growth influences that can be caused by the interfering strain on the senders or receivers (see Fig. S7). Next, we both experimentally and theoretically examine the influence of AiiA-mediated interference in spatially distributed networks of cells.

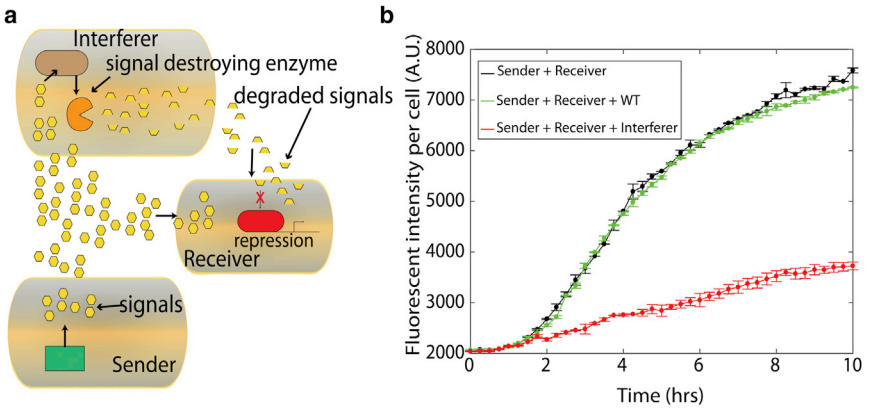

FIGURE 2 (*a*) To quantify the impact of interference on signal exchange, a third strain is added to the system that produces the enzyme AiiA, a lactonase that cleaves AHL signal. (*b*) Addition of the interference strain to the sender-and-receiver community reduces the fluorescence intensity per cell of the receiver strain. Here, the negative control shows that the addition of the wild-type yields a curve similar to the case of no interference. Error bars show the standard deviation of three replicate measurements. To see this figure in color, go online.

Signal destruction leads to finite and tunable zones of activation in spatial networks

The interference strain was added to the plate-based assay to quantify the influence of signal destruction on the signaling dynamics. The interference strain was added to the lawn of receiver cells, as depicted in Fig. 3 *a*. Different amounts of the interfering strains were titrated into the receiver cells to measure the robustness of signal propagation to a variable level of interference.

Fig. 3 *b* shows the impact of different levels of interference on signaling dynamics. The no-interference data from Fig. 1 *c* is shown for reference. As the level of interference increased, we observed a slight delay in quorum-sensing activation. Additionally, the system only activated up to a finite distance. For example, at a normalized level of interference of 0.9, receiver cells at a distance of 2.3 mm activated at ~5.5 h. The experiment continued to run for a total time of 16 h, and activation beyond 2.3 mm was not observed (see Fig. S8). The radius of the activation zone was inversely proportional to the level of interference. As seen in Fig. S7, there are no significant growth influences between the strains. To confirm that this effect was due to production of the AiiA enzyme, in control experiments, a wild-type strain that does not produce AiiA was substituted for the interference strain (Fig. S9).

Modeling the impact of signal destruction on signal propagation

A model for signal exchange in the presence of interference was derived to further explore the ability of signal destruction to limit the zone of activation. Our model, based on previously reported models from (27) and (39) accounts for the growth of the sender strain, the receiver strain, and the interference strain. All three strains follow the logistic growth equation,

$$\frac{\partial n}{\partial t} = \mu\, n\left(1 - \frac{n_{\text{Total}}}{s}\right), \tag{1}$$

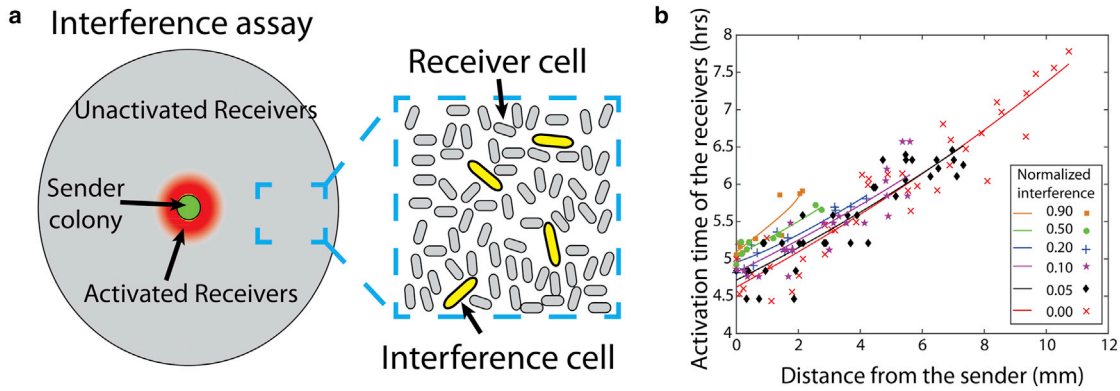

FIGURE 3 (*a*) Introducing the AiiA cells in the plate-assay setup. (*b*) Activation time versus distance from the sender plot for variable levels of interference. The number of interference cells in the assay is normalized to the number of cells in 100 μL of cells in a culture with an absorbance of 1.0 at 600 nm. Curves show an exponential fit to demonstrate qualitative trends in the data. Experiments were run for 16 h, much longer than the time needed to observe the maximum radius of activation.

where μ is the growth rate constant, n is the cell density, n_{Total} is the total cell density (senders + receivers + interferers), and s is the maximal cell density in the system. All three strains use the same *E. coli* host and were shown to have similar growth characteristics (see Fig. S7). Fig. S7 shows that there are no growth influences on the sender and the receivers when cocultured with the interferer.

Several models have been used to describe quorum-sensing signaling (27–30,39–41), including signaling in the presence of signal destruction (27). The dynamics of the AHL signal, [AHL], by the sender strain can be described by the equation

$$\frac{\partial[\text{AHL}]}{\partial t} = D_{\text{AHL}}\nabla^2[\text{AHL}] + n_{\text{AHL}}\left(\rho_{\text{AHL}}\frac{[\text{AHL}]^{m_1}}{[\text{AHL}]^{m_1}+\theta_1^{m_1}} + \rho_{\text{b1}}\right) - \gamma_1[\text{AHL}] - \gamma_2[\text{AiiA}]\frac{[\text{AHL}]^{m_2}}{[\text{AHL}]^{m_2}+\theta_2^{m_2}}, \quad (2)$$

where D_{AHL} is the diffusion coefficient for the signal, n_{AHL} is the cell density of the senders, ρ_{AHL} is the maximal production rate of the AHL per cell, ρ_{b1} is the basal level of AHL production, θ_i represents the concentration of the signal at half maximum activity, m_i represents the cooperative coefficients, γ_1 is the basal rate of signal degradation in media (39,42), γ_2 is the rate of signal degradation due to the AiiA, and [AiiA] is the concentration of AiiA signal. The Hill's function represents a threshold amount of signal needed to activate quorum sensing up to a maximum production rate.

The change in the amount of AiiA is described by

$$\frac{\partial[\text{AiiA}]}{\partial t} = n_{\text{AiiA}}\left(\rho_{\text{AiiA}}\frac{[\text{AHL}]^{m_3}}{[\text{AHL}]^{m_3}+\theta_3^{m_3}} + \rho_{\text{b2}}\right) - \gamma_3[\text{AiiA}], \quad (3)$$

where, ρ_{AiiA} is the maximum production rate of the AiiA per cell, ρ_{b2} is the basal level of AiiA production, n_{AiiA} is the cell density of the AiiA cells, and γ_3 is the basal rate of AiiA degradation. The values of all the parameters are given in Table 1. Given the timescale of our simulations, we assume that the degradation rate of the AiiA will be low and set it to the degradation rate of the AHLs. In the Supporting Material, we estimate the number of AiiA molecules per cell and conclude that the production rates used give a reasonable level of protein per cell.

In the simulations, we solve the equations using the finite-difference method. The interference strain is evenly distributed in the simulation grid at various loading densities. Activation occurs at a distance X when the concentration of AHL signal at that point reaches the threshold concentration. Growth-rate constants were experimentally obtained, as shown in Fig. S7 *A*. Additional parameters were reported in previous studies.

TABLE 1 Values of Parameters in Eqs. 1–3

Parameter	Value
μ	1.50 h^{-1} (experimentally calculated)
s	10^9 cells per mL
D_{AHL}	1.764 mm^2 h^{-1} (40)
ρ_{AHL}	2.3×10^{-9} nmol h^{-1} per cell (39)
ρ_{b1}	2.3×10^{-10} nmol h^{-1} per cell (39)
θ_1	70 nM (39)
θ_2	70 nM (32)
m_1	2.5 (32)
m_2	2.5 (32)
γ_1	0.005545 h^{-1} (39)
γ_2	0.01 h^{-1} (27)
ρ_{AiiA}	2.3×10^{-9} nmol h^{-1} per cell
ρ_{b2}	2.3×10^{-10} nmol h^{-1} per cell
γ_3	0.005545 h^{-1}
θ_3	70 nM (39)
m_3	2.5 (32)

As shown in Fig. 4 *a*, simulations of the dynamics of activation in the plate-based assay qualitatively matched activation profiles from the experimental measurements at steady state. The transient behavior in Fig. 3 *b* was compared to the simulation results in Fig. S10. Predicted steady-state activation diameters were closed to experimental measurements, although simulations reached the steady-state diameter 20–30 min earlier than in experiments. The delayed activation in experiment could be due to processes such as fluorescent protein folding and maturation and time delays in signal processing, which were not included in the model. As shown in Fig. 4 *b*, model predictions for the plate-based assay are in close agreement with experimental results (see Fig. S11 for simulation predictions of the well-mixed system). As the percentage of interference strain increased, the activation zone shrank from 10 mm down to 2 mm, demonstrating that the number of interfering cells within the system tunes the radius of activation. As in experiments, simulations were run for 16 h, much longer than the time needed to reach steady-state activation profiles. In these experiments, expression of *aiiA* is regulated by the AHL quorum-sensing signal, although simulations and experiments shown in Fig. S12 demonstrate that strains without AHL-dependent *aiiA* expression exhibit similar activation dynamics.

In simulations and experiments we varied the number of cells in the sender colony and observed that when the number of cells in the sender strain was increased or decreased by a factor of 5, the activation range curve shifted (Fig. 4 *c*). Together, the ratio of sender to interference strains dictates the spatial extent of activation. To further explore the parameters that dictate the dynamics of the activation zone, in simulations, we varied multiple model parameters, including the diffusion coefficient and the degradation of AHL due to the media (Figs. S13 and S14). We observe that the major contributors to the activation zone are the diffusion of the AHLs and the degradation of the AHL by the interferer. The production rate of the AHLs by the senders weakly

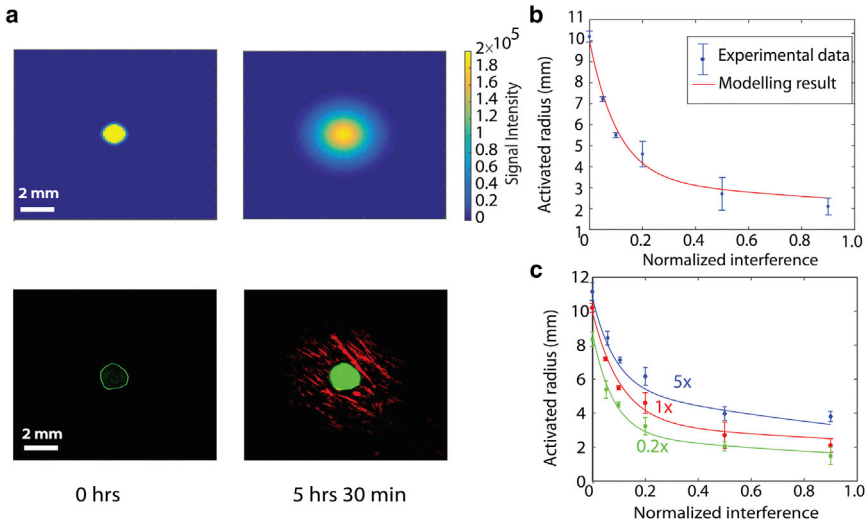

FIGURE 4 (*a*) A model using Eqs. 1–3 simulates receiver-cell activation in the plate-based assay (*top*), and the experimental comparison is shown below. Here, the normalized interference level is 0.9. (*b*) The maximal activated radius of the receivers versus the normalized number of interference cells. The experimental measurements (*dots*) agreed with model predictions (*line*). (*c*) Theoretical predictions and experimental data points for the activation radius when the number of sender cells is increased by 5× or decreased to 0.2×. Error bars show the standard deviation of three replicate measurements. To see this figure in color, go online.

influences the activation radius, as shown in Fig. S14 *A*. In Fig. S15, through simulations, we demonstrate that the potential growth interactions between the strains and internalization of the signal by non-receiver strains can produce a similar limitation in the activation zone. Although theoretically hypothesized, the changes to the activation zone by these parameters would need to be experimentally validated.

CONCLUSIONS

We have demonstrated that signal interference with a bacterial communication pathway through signal destruction creates a finite region of activation around a colony of signal emitting cells. Similar spatial activity patterns have been programmed using external chemical gradients or synthetic signaling circuits (19,22,24,43). Here a plate-based experimental assay was implemented to quantify the influence of interference on signal transduction in a spatially heterogeneous system. The assay measurements were supported by a reaction-diffusion simulation of signal dynamics, demonstrating the utility of such models in predicting signal exchange in systems with complex geometries that could not easily be analyzed experimentally.

Both the theoretical and experimental results revealed the capability of tuning the system-level parameters of a multi-strain bacterial community. By adjusting the amount of interference strain, the zone of activation was tunable from 2 to 10 mm. Theoretical predictions and experimental results shown in Fig. 4 *c* demonstrate that parameters such as the number of sender cells also modulated the radius of activation. Parameters including the diffusion coefficient of the signal, degradation and production rates of the signal, and cell growth rates were modulated in simulations, predicting that the area of activation was most sensitive to signal transport and degradation rates. Experimental validation of these predictions is needed. Similar theoretical models of signaling have explored the network parameters that regulate bacterial pattern formation (20,26). Such strategies for adjusting the dynamics of multispecies interactions might prove useful for programming the activity of synthetic communities.

Recent interest in engineering microbial communities to perform complex tasks (32,37,44), such as in nanoscale synthesis and biomedical applications (19,45–47), call for new experimental techniques to control the network-level behavior of microbial communities (45,48–50). Although characterization of diverse communities often focuses on well-mixed systems, nonlinearities in the interactions can result in unexpected outcomes, particularly in spatially heterogeneous systems (33,51,52). The plate-based assay developed here may prove useful to quantify the outputs of spatially distributed, multispecies networks (53). Such approaches identify control parameters, such as the level of signal destruction shown here, that strongly determine global behaviors. These experiments, in conjunction with theoretical models, will enable us to understand and predict the parameters that determine community behavior in multispecies bacterial communities.

Our results suggest that in natural systems even low levels of interference will modulate the dynamics of signal propagation, and hence the functional outputs of the community. Many natural systems are spatially heterogeneous, and the consequences of specific spatial distributions could be predicted in simulations. It remains unclear to what extent interference constrains signaling to local areas. Recent studies have examined quorum sensing that occurs locally within small populations (54,55), but there are examples of long-distance coordination of cellular behaviors known to be coordinated by signal exchange (5,56). Given the number of quorum-quenching and signal-interference mechanisms present in natural communities (13,16,17), future work should examine the contributions of different types of interference beyond signal destruction, such as receptor

blocking through competitive binding, in shaping global signaling responses.

SUPPORTING MATERIAL

Supporting Materials and Methods and fifteen figures are available at http://www.biophysj.org/biophysj/supplemental/S0006-3495(17)30105-4.

AUTHOR CONTRIBUTIONS

K.P.S. performed the research, analyzed data, and wrote the article; P.C. performed the research and wrote the article; J.Q.B. designed the research, analyzed data, and wrote the article.

ACKNOWLEDGMENTS

This work was supported by Office of Naval Research award number N00014-15-1-2573 and a Defense Advanced Research Projects Agency Young Faculty Award.

REFERENCES

1. de Kievit, T. R., and B. H. Iglewski. 2000. Bacterial quorum sensing in pathogenic relationships. *Infect. Immun.* 68:4839–4849.
2. Li, Y.-H., and X. Tian. 2012. Quorum sensing and bacterial social interactions in biofilms. *Sensors (Basel).* 12:2519–2538.
3. Yang, Q., and T. Defoirdt. 2015. Quorum sensing positively regulates flagellar motility in pathogenic *Vibrio harveyi*. *Environ. Microbiol.* 17:960–968.
4. Boedicker, J., and K. Nealson. 2016. INVITED: microbial communication via quorum sensing. *IEEE Trans. Mol. Biol. Multi-Scale Commun.* 1:310–320.
5. Nealson, K. H., and J. W. Hastings. 2006. Quorum sensing on a global scale: massive numbers of bioluminescent bacteria make milky seas. *Appl. Environ. Microbiol.* 72:2295–2297.
6. Miller, M. B., and B. L. Bassler. 2001. Quorum sensing in bacteria. *Annu. Rev. Microbiol.* 55:165–199.
7. Cornforth, D. M., R. Popat, …, S. P. Brown. 2014. Combinatorial quorum sensing allows bacteria to resolve their social and physical environment. *Proc. Natl. Acad. Sci. USA.* 111:4280–4284.
8. Sifri, C. D. 2008. Healthcare epidemiology: quorum sensing: bacteria talk sense. *Clin. Infect. Dis.* 47:1070–1076.
9. Heilmann, S., S. Krishna, and B. Kerr. 2015. Why do bacteria regulate public goods by quorum sensing?—How the shapes of cost and benefit functions determine the form of optimal regulation. *Front. Microbiol.* 6:767.
10. Kavanaugh, J. S., M. Thoendel, and A. R. Horswill. 2007. A role for type I signal peptidase in *Staphylococcus aureus* quorum sensing. *Mol. Microbiol.* 65:780–798.
11. Heurlier, K., V. Dénervaud, and D. Haas. 2006. Impact of quorum sensing on fitness of *Pseudomonas aeruginosa*. *Int. J. Med. Microbiol.* 296:93–102.
12. Darch, S. E., S. A. West, …, S. P. Diggle. 2012. Density-dependent fitness benefits in quorum-sensing bacterial populations. *Proc. Natl. Acad. Sci. USA.* 109:8259–8263.
13. Rampioni, G., L. Leoni, and P. Williams. 2014. The art of antibacterial warfare: deception through interference with quorum sensing-mediated communication. *Bioorg. Chem.* 55:60–68.
14. Williams, P., K. Winzer, …, M. Cámara. 2007. Look who's talking: communication and quorum sensing in the bacterial world. *Philos. Trans. R. Soc. Lond. B Biol. Sci.* 362:1119–1134.
15. Grandclément, C., M. Tannières, …, D. Faure. 2016. Quorum quenching: role in nature and applied developments. *FEMS Microbiol. Rev.* 40:86–116.
16. Dong, Y. H., L. Y. Wang, and L.-H. Zhang. 2007. Quorum-quenching microbial infections: mechanisms and implications. *Philos. Trans. R. Soc. Lond. B Biol. Sci.* 362:1201–1211.
17. Pérez, P. D., J. T. Weiss, and S. J. Hagen. 2011. Noise and crosstalk in two quorum-sensing inputs of *Vibrio fischeri*. *BMC Syst. Biol.* 5:153.
18. McClean, K. H., M. K. Winson, …, P. Williams. 1997. Quorum sensing and *Chromobacterium violaceum*: exploitation of violacein production and inhibition for the detection of *N*-acylhomoserine lactones. *Microbiology.* 143:3703–3711.
19. Basu, S., Y. Gerchman, …, R. Weiss. 2005. A synthetic multicellular system for programmed pattern formation. *Nature.* 434:1130–1134.
20. Cao, Y., M. D. Ryser, …, L. You. 2016. Collective space-sensing coordinates pattern scaling in engineered bacteria. *Cell.* 165:620–630.
21. Masiello, C. A., Y. Chen, …, J. J. Silberg. 2013. Biochar and microbial signaling: production conditions determine effects on microbial communication. *Environ. Sci. Technol.* 47:11496–11503.
22. Sohka, T., R. A. Heins, …, M. Ostermeier. 2009. An externally tunable bacterial band-pass filter. *Proc. Natl. Acad. Sci. USA.* 106:10135–10140.
23. Kong, W., A. E. Blanchard, …, T. Lu. 2016. Engineering robust and tunable spatial structures with synthetic gene circuits. *Nucleic Acids Res.* Epub ahead of print. http://dx.doi.org/10.1093/nar/gkw1045.
24. Liu, C., X. Fu, …, J.-D. Huang. 2011. Sequential establishment of stripe patterns in an expanding cell population. *Science.* 334:238–241.
25. Wang, Y., Y. Dai, …, S. Chen. 2007. Effects of quorum sensing autoinducer degradation gene on virulence and biofilm formation of Pseudomonas aeruginosa. *Sci. China C. Life Sci.* 50:385–391.
26. Borek, B., J. Hasty, and L. Tsimring. 2016. Turing patterning using gene circuits with gas-induced degradation of quorum sensing molecules. *PLoS One.* 11:e0153679.
27. Danino, T., O. Mondragón-Palomino, …, J. Hasty. 2010. A synchronized quorum of genetic clocks. *Nature.* 463:326–330.
28. Langebrake, J. B., G. E. Dilanji, …, P. De Leenheer. 2014. Traveling waves in response to a diffusing quorum sensing signal in spatially-extended bacterial colonies. *J. Theor. Biol.* 363:53–61.
29. Dilanji, G. E., J. B. Langebrake, …, S. J. Hagen. 2012. Quorum activation at a distance: spatiotemporal patterns of gene regulation from diffusion of an autoinducer signal. *J. Am. Chem. Soc.* 134:5618–5626.
30. Trovato, A., F. Seno, …, A. Squartini. 2014. Quorum vs. diffusion sensing: a quantitative analysis of the relevance of absorbing or reflecting boundaries. *FEMS Microbiol. Lett.* 352:198–203.
31. Molina, L., F. Constantinescu, …, G. Défago. 2003. Degradation of pathogen quorum-sensing molecules by soil bacteria: a preventive and curative biological control mechanism. *FEMS Microbiol. Ecol.* 45:71–81.
32. Kong, W., V. Celik, …, T. Lu. 2014. Programming the group behaviors of bacterial communities with synthetic cellular communication. *Bioresour. Bioprocess.* 1:24.
33. Servinsky, M. D., J. L. Terrell, …, W. E. Bentley. 2016. Directed assembly of a bacterial quorum. *ISME J.* 10:158–169.
34. Weitz, M., A. Mückl, …, F. C. Simmel. 2014. Communication and computation by bacteria compartmentalized within microemulsion droplets. *J. Am. Chem. Soc.* 136:72–75.
35. Choi, W. S., D. Ha, …, T. Kim. 2011. Synthetic multicellular cell-to-cell communication in inkjet printed bacterial cell systems. *Biomaterials.* 32:2500–2507.
36. Marchand, N., and C. H. Collins. 2013. Peptide-based communication system enables *Escherichia coli* to *Bacillus megaterium* interspecies signaling. *Biotechnol. Bioeng.* 110:3003–3012.
37. Chen, Y., J. K. Kim, …, M. R. Bennett. 2015. SYNTHETIC BIOLOGY. Emergent genetic oscillations in a synthetic microbial consortium. *Science.* 349:986–989.

38. Zhang, F., A. Kwan, …, G. M. Süel. 2015. A synthetic quorum sensing system reveals a potential private benefit for public good production in a biofilm. *PLoS One.* 10:e0132948.

39. Fekete, A., C. Kuttler, …, A. Hartmann. 2010. Dynamic regulation of N-acyl-homoserine lactone production and degradation in *Pseudomonas putida* IsoF. *FEMS Microbiol. Ecol.* 72:22–34.

40. Stewart, P. S. 2003. Diffusion in biofilms. *J. Bacteriol.* 185:1485–1491.

41. Ramalho, T., A. Meyer, …, F. C. Simmel. 2016. Single cell analysis of a bacterial sender-receiver system. *PLoS One.* 11:e0145829.

42. Englmann, M., A. Fekete, …, P. Schmitt-Kopplin. 2007. The hydrolysis of unsubstituted *N*-acylhomoserine lactones to their homoserine metabolites. Analytical approaches using ultra performance liquid chromatography. *J. Chromatogr. A.* 1160:184–193.

43. Payne, S., B. Li, …, L. You. 2013. Temporal control of self-organized pattern formation without morphogen gradients in bacteria. *Mol. Syst. Biol.* 9:697.

44. Tamsir, A., J. J. Tabor, and C. A. Voigt. 2011. Robust multicellular computing using genetically encoded NOR gates and chemical "wires". *Nature.* 469:212–215.

45. Brenner, K., L. You, and F. H. Arnold. 2008. Engineering microbial consortia: a new frontier in synthetic biology. *Trends Biotechnol.* 26:483–489.

46. Coker, V. S., N. D. Telling, …, J. R. Lloyd. 2009. Harnessing the extracellular bacterial production of nanoscale cobalt ferrite with exploitable magnetic properties. *ACS Nano.* 3:1922–1928.

47. Chen, A. Y., Z. Deng, …, T. K. Lu. 2014. Synthesis and patterning of tunable multiscale materials with engineered cells. *Nat. Mater.* 13:515–523.

48. Shong, J., M. R. Jimenez Diaz, and C. H. Collins. 2012. Towards synthetic microbial consortia for bioprocessing. *Curr. Opin. Biotechnol.* 23:798–802.

49. Zengler, K., and B. O. Palsson. 2012. A road map for the development of community systems (CoSy) biology. *Nat. Rev. Microbiol.* 10:366–372.

50. Johns, N. I., T. Blazejewski, …, H. H. Wang. 2016. Principles for designing synthetic microbial communities. *Curr. Opin. Microbiol.* 31:146–153.

51. Ratzke, C., and J. Gore. 2016. Self-organized patchiness facilitates survival in a cooperatively growing *Bacillus subtilis* population. *Nat. Microbiol.* 1:16022.

52. Kastrup, C. J., J. Q. Boedicker, …, R. F. Ismagilov. 2008. Spatial localization of bacteria controls coagulation of human blood by 'quorum acting'. *Nat. Chem. Biol.* 4:742–750.

53. Straight, P. D., J. M. Willey, and R. Kolter. 2006. Interactions between *Streptomyces coelicolor* and *Bacillus subtilis*: role of surfactants in raising aerial structures. *J. Bacteriol.* 188:4918–4925.

54. Connell, J. L., J. Kim, …, M. Whiteley. 2014. Real-time monitoring of quorum sensing in 3D-printed bacterial aggregates using scanning electrochemical microscopy. *Proc. Natl. Acad. Sci. USA.* 111:18255–18260.

55. Kim, H. J., J. Q. Boedicker, …, R. F. Ismagilov. 2008. Defined spatial structure stabilizes a synthetic multispecies bacterial community. *Proc. Natl. Acad. Sci. USA.* 105:18188–18193.

56. Prindle, A., P. Samayoa, …, J. Hasty. 2011. A sensing array of radically coupled genetic "biopixels". *Nature.* 481:39–44.

Biophysical Journal, Volume *112*

Supplemental Information

Signal Destruction Tunes the Zone of Activation in Spatially Distributed Signaling Networks

Kalinga Pavan Silva, Prithiviraj Chellamuthu, and James Q. Boedicker

Plasmids

Plasmids to create the sender and interferer were obtained from Addgene. The plasmids were inserted into *E. coli Dh5alpha.* The plasmids in the sender and interferer were based on study (1).

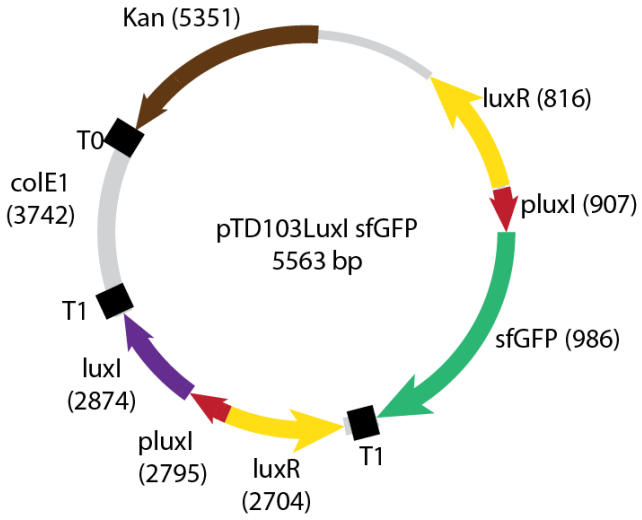

Figure S1: The map for the plasmid in the sender. *luxI* encodes for the production of the AHL 3-oxo-c6-HSL. *luxR* encodes for the production of the receptor protein LuxR. Once the AHL binds to the LuxR protein it could bind to the *pluxI* promoter and activate the expression of the genes *luxI*, *luxR* and *sfGFP*.

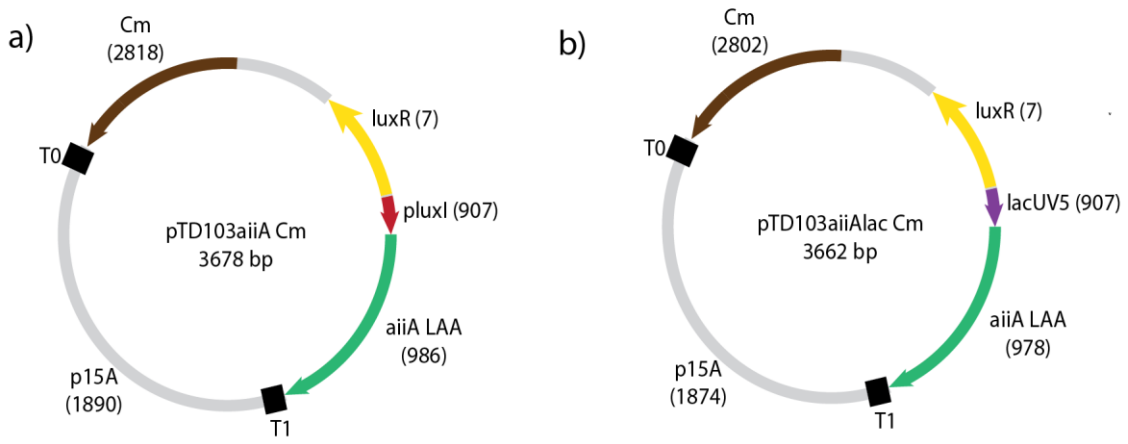

Figure S2: The map for the plasmid in the Interferer (a). regulated under the *pluxI* promoter (b). constitutive under the *lacUV5* promoter. For the regulated interferer strain, the AHLs diffusing from the sender will bind to the LuxR protein, and activate the *pluxI* promoter and express the *aiiA* gene while for the constitutive interferer strain the *aiiA* gene will be produced constitutively. The *aiiA* gene will encode for the production of the degradative enzyme AiiA.

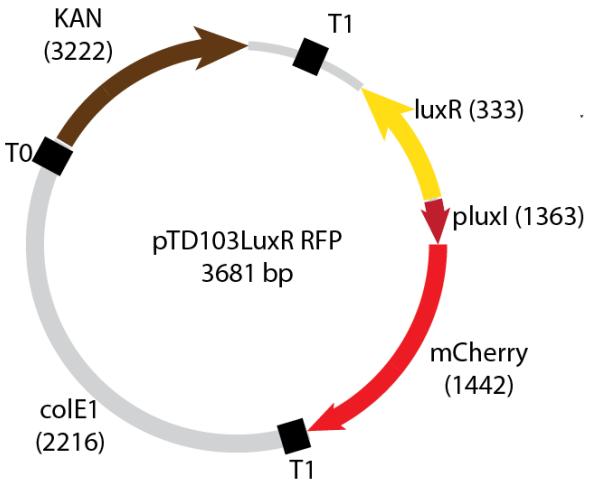

Figure S3: The map for the plasmid in the receiver. The *pluxI* promoter will activate due to the diffusing AHLs from the sender. Once activated, LuxR and the mCherry fluorescent protein will be produced. We constructed the receiver, based on the ptD103 plasmid. The *luxI* and *sfGFP* genes were deleted from the ptD103luxI sfGFP plasmid and the *mCherry* sequence was added in place of the *sfGFP* gene.

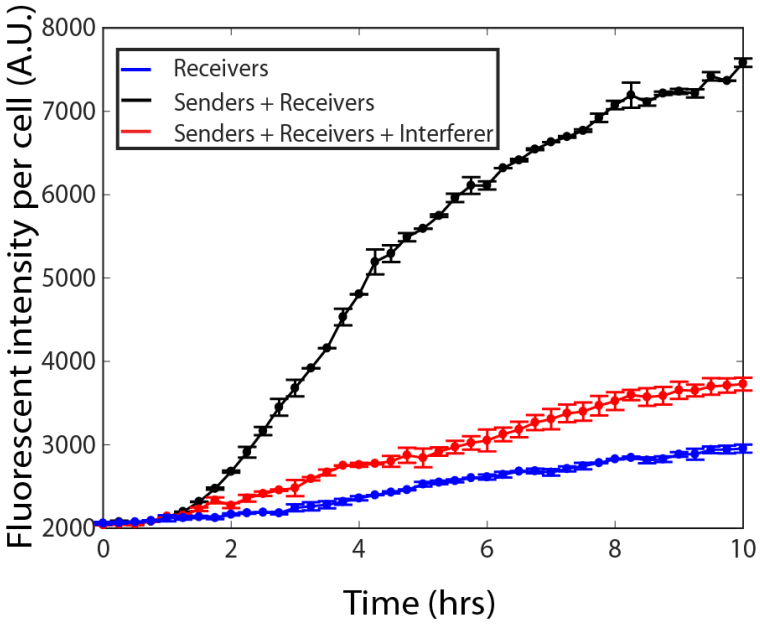

Figure S4: The change in fluorescent intensity per cell of the receivers as a result of coculture with the sender strain or the sender strain and the interferer strain. Fluorescent intensity was measured in the plate reader at 37 °C as described in the main text.

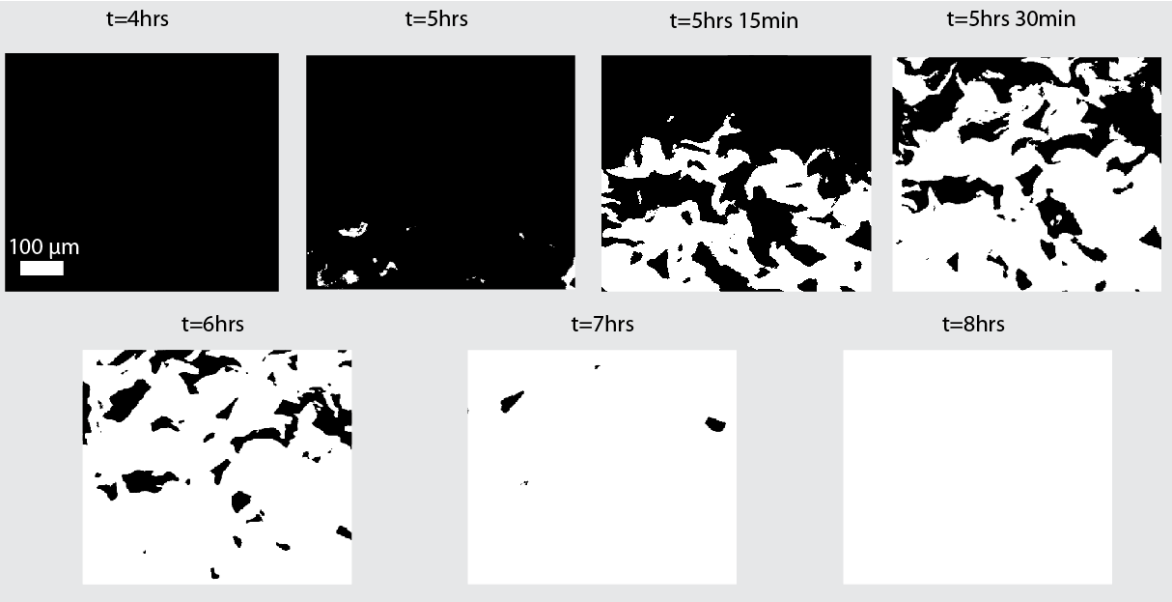

Figure S5: Analysis of growth of the artivation for the case of no interference. At the threshold (10% of the maximal pixel value for the microscope), we see clear activation (white) of the receivers at a distance of 2 mm (bottom edge of the frame) from the senders. The images here are taken from the microscope and the size of each frame is 750 µm. The receiver activates from bottom to top.

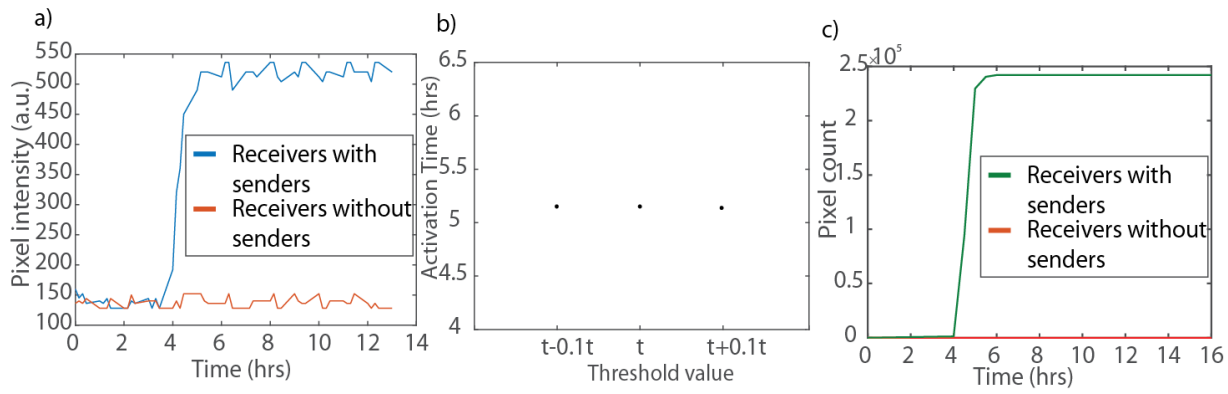

Figure S6: Sensitivity of results to the activation threshold value. a) The pixel intensity of the receivers over time at a distance 2 mm from the sender and in a negative control of receivers without added sender. b) The calculated activation times when we change the threshold was raised or lowered by 10%. c) Upon applying the threshold, the number of pixels above threshold was counted for receiver cells 2 mm from the sender and in the no sender negative control.

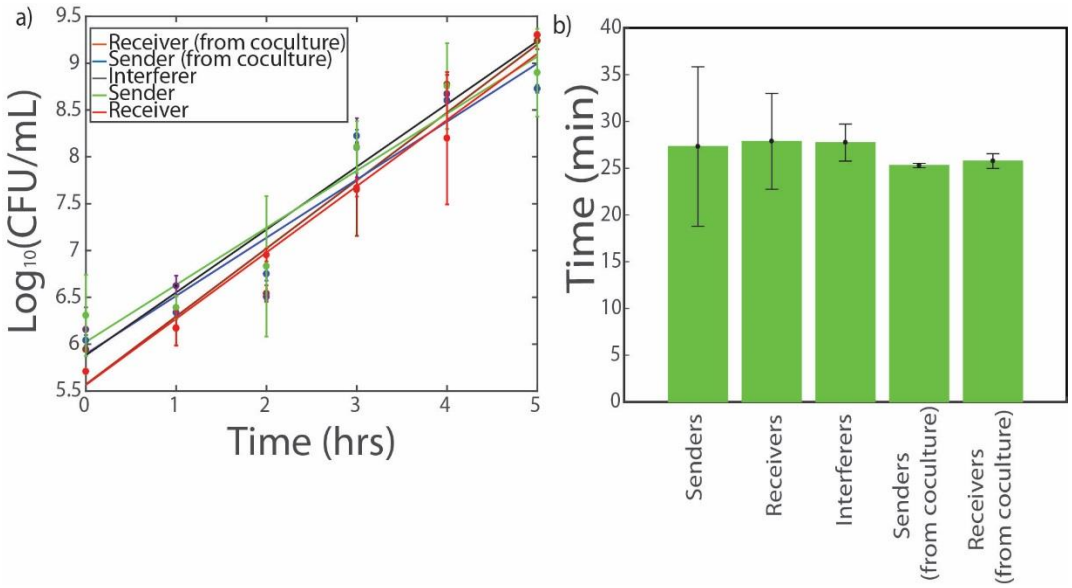

Figure S7: Addition of the interferer strain did not significantly change the doubling time of the sender or the receiver. a) Growth curves for the sender, receiver, and interferer strain alone and in coculture. In coculture experiments, selective plating enabling tracking of individual species. b). Fits to the linear doubling times of the sender, receiver, and interference strains. The errorbars show standard deviation from four replicates. A standard unpaired t test was used to calculate the two tailed p value. Comparisons between the doubling times of the senders or receivers with and without addition of the interferer had $p > 0.5$.

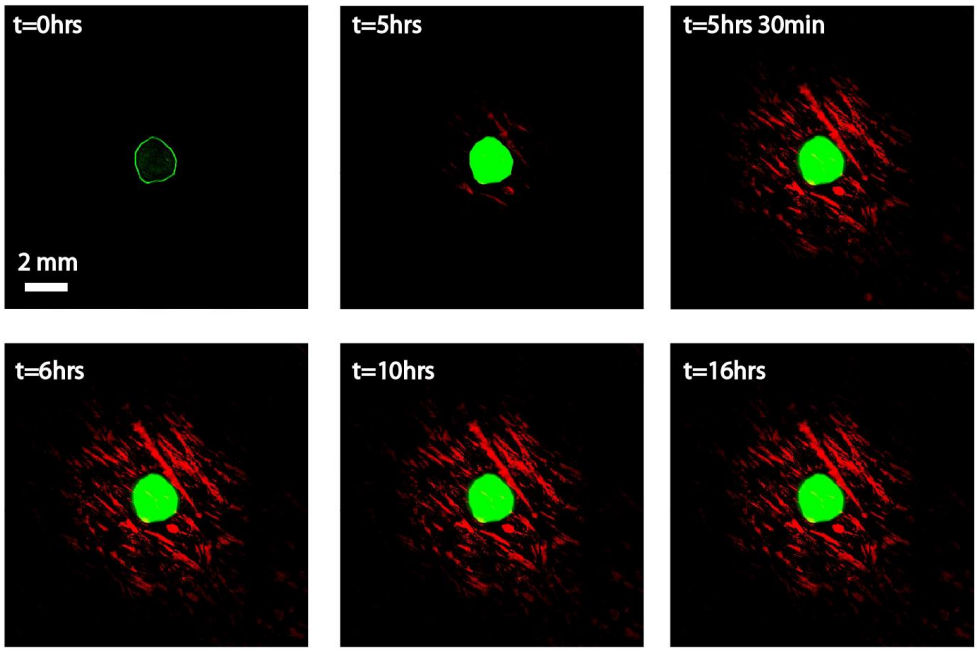

Figure S8: The plate assay experiment shown here for normalized interference level 0.9 shows that the activation of the receivers stop at a distance 2.3 mm. The experiments were done for 16 hours, and no propagation in the activation was observed. The dark areas within activated regions are the result of variability in the initial distribution of receiver cells

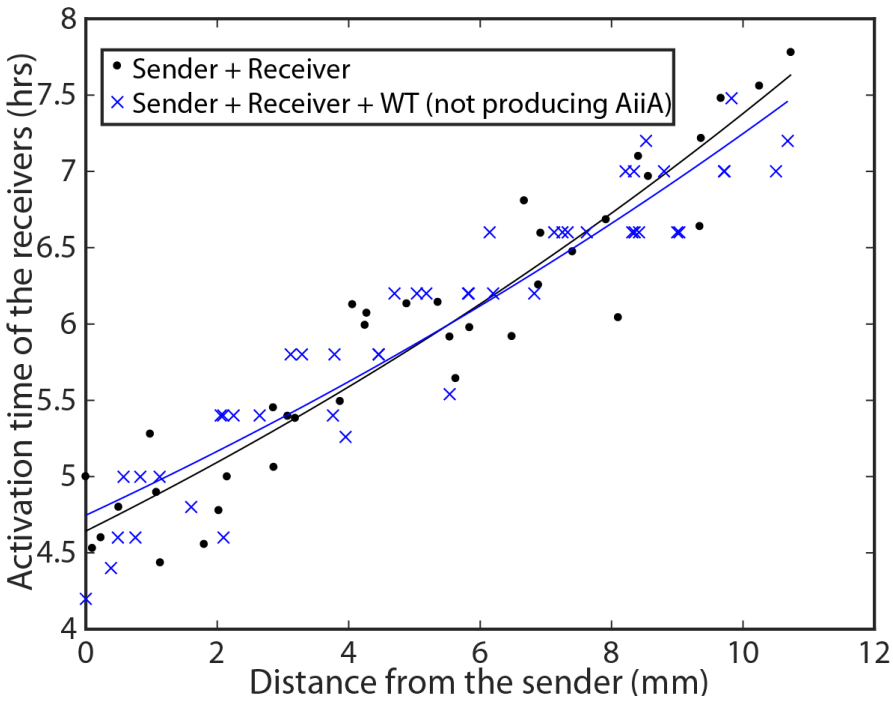

Figure S9: Control experiment compares the activation dynamics of the sender and receiver alone (black dots) or when paired with the wild type (WT) host that does not produce the AiiA enzymes (blue X's). Plate-assay setup as described in the main text.

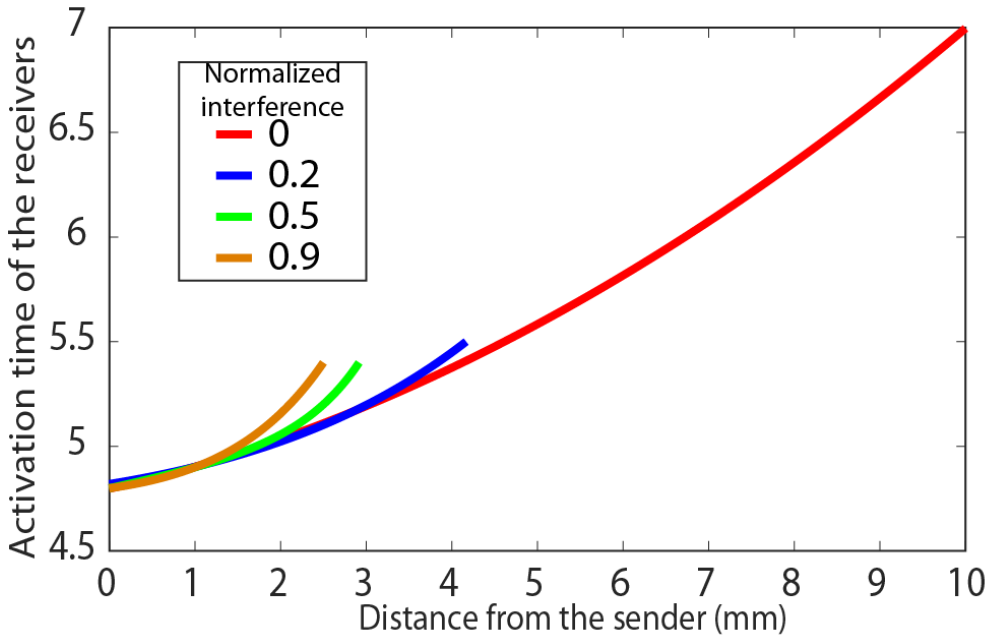

Figure S10: Simulation results for the activation time vs. distance for the receivers

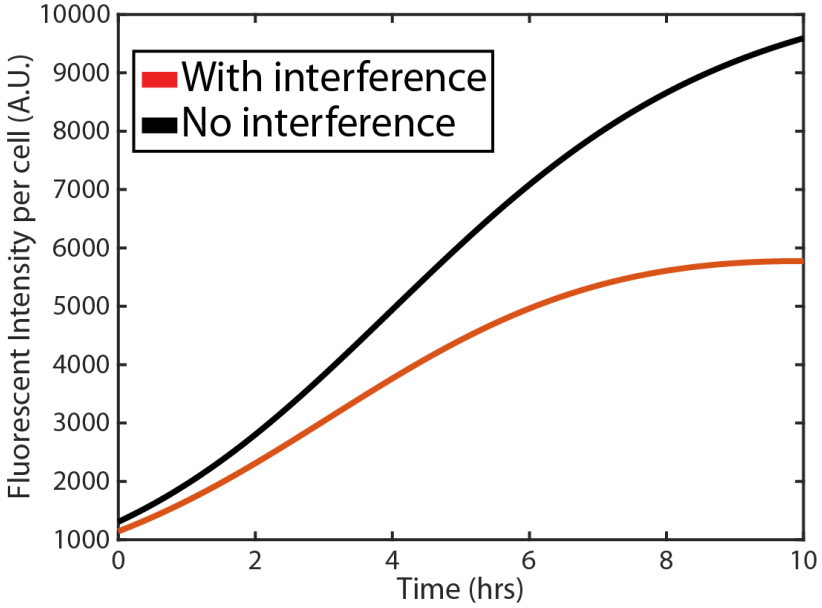

Figure S11: The model predictions made for the changes in the fluorescent intensity per receiver cell, with and without the AiiA species. Here we obtain the concentration profiles of the AHLs in a well-mixed setup and convert it to the fluorescent intensity per cell by multiplying with an arbitrary value.

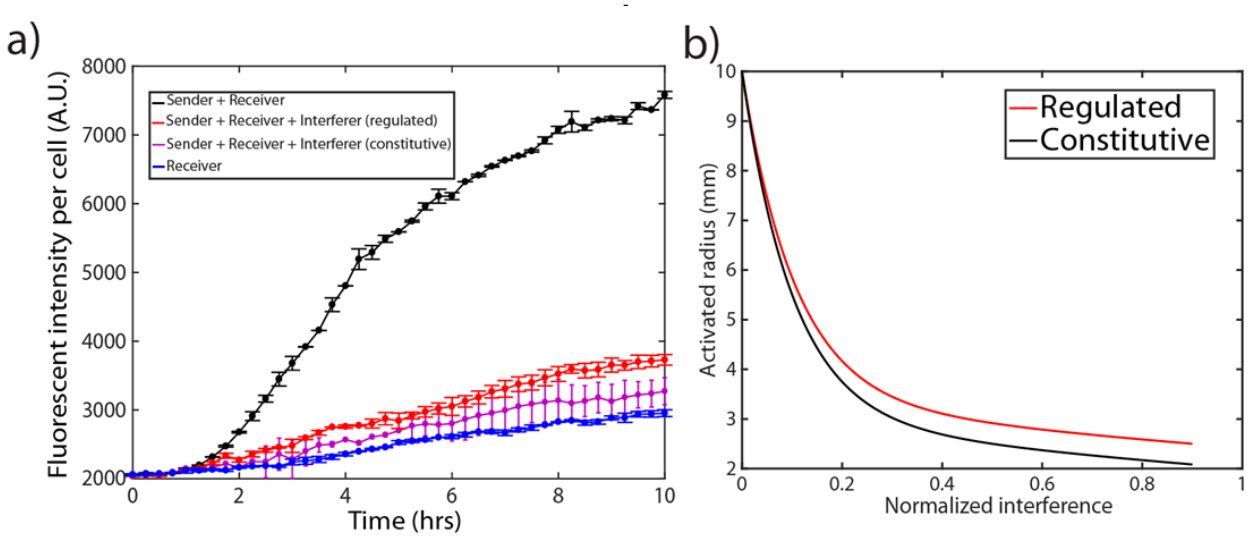

Figure S12: Regulated vs constitutive production of AiiA in the interference strain. (a). Plate reader experiments shows that the constitutive interferer (purple) yields a similar response to the regulated interferer (red). (b). Simulations confirms that the plate assay setup will yield a similar response to the regulated case. To simulate the constitutive production of AiiA, we delete the Hill's coefficient appearing in equation {3} such that the AiiA strain will constitutively produce the AiiA at a constant rate of production of 2.3×10^{-9} nM hrs^{-1} per cell.

Calculation of the number of proteins per cell for the production rate of AiiA

In this section we will justify that the production rate assumed for AiiA (2.3×10^{-10} nmol hrs^{-1} per cell) in the modelling is reasonable. The system is simulated for 10 hours.

At t=10 hours, the amount of AiiA per cell can be estimated as: 2.3×10^{-10} nmol hrs^{-1} per cell x 10 hours= 2.3×10^{-9} nmol per cell or 2.3×10^{-18} mol per cell.

In molecules, AiiA per cell would be: 2.3×10^{-18} mol per cell x 6.022×10^{23} molecules/mol ~ 10^{6} molecules per cell.

Hence, we estimate on the order of 10^{6} AiiA proteins produced per cell at t=10 hours in the simulations, which is within the range of the standard number of proteins per bacterial cell (2), particularly for a production from a gene encoded on a plasmid.

Calculating the fluorescence in a mixed culture using the plate reader

In this section our objective is to calculate the fluorescence of a species in a mixed culture. In the mixed culture, there will be two species, one with a particular fluorescence (ex: RFP) and the other strain will not have the same fluorescence. We experimentally measure the total fluorescence of the mixture using a plate-reader.

We define the following terms,

Fluorescence readout from the plate reader = Fl;

Number of cells = n;

Optical density readout from the plate reader = O;

Background fluorescence per cell= α;

Fluorescence per protein = ω;

Number of fluorescent protein per cell = f;

Absorbance of light per cell = β;

Let's consider a general case where species A produces the fluorescence (ex:RFP) and species B doesn't produce any or the same fluorescence as species A. There will be a background fluorescence due to the light scattering off the edges of the cell.

First we will consider the total fluorescence of the mixed culture;

$Fl_{total} = n_A f \omega + n_A \alpha_A + n_B \alpha_B + Fl_m$ **{4}**

Where, Fl_m is the background fluorescence of the media.

The corresponding optical density will be;

$O_{total} = n_A \beta + n_B \beta + O_m$ **{5}**

Where, O_m is the background fluorescence of the media.

If species B is grown in a single culture the fluorescence of species B will be;

$Fl_B = n_B \alpha_B + Fl_m$ **{6}**

The corresponding optical density of species B will be;

$O_B = n_B \beta + O_m$ **{7}**

Since we use E. *coli* (DH5alpha, NEB10beta) cells for all of the different species in our study, we assume that the background fluorescence per cell in all the cells is the same. ($\alpha_A = \alpha_B = \alpha_1$)

Now, the total fluorescence of the mixed culture for all the cells,

$$\frac{Fl_{total} - Fl_m}{O_{total} - O_m} = \frac{n_A f \omega + n_A \alpha_1 + n_B \alpha_1}{n_A \beta + n_B \beta} \quad \textbf{\{8\}}$$

The total fluorescence of species B in the single culture,

$$\frac{Fl_B - Fl_m}{O_B - O_m} = \frac{n_B \alpha_1}{n_B \beta} \quad \textbf{\{9\}}$$

Now lets define Δ_A ={8} - {9}

$$\Delta_A = \frac{n_A f \omega + n_A \alpha_1 + n_B \alpha_1}{n_A \beta + n_B \beta} - \frac{\alpha_1}{\beta}$$

$$= \frac{n_A\, f\, \omega + n_A\, \alpha_1 + n_B\, \alpha_1 - (n_A + n_B)\alpha_1}{(n_A + n_B)\, \beta}$$

$$= \frac{n_A\, f\, \omega}{(n_A + n_B)\beta} \qquad \textbf{\{10\}}$$

Now from **{5};**

$$(n_A + n_B)\beta = O_{total} - O_m \qquad \textbf{\{11\}}$$

$\emptyset_A = n_A\, f\, \omega$, is the total fluorescence of the species A in the mixture.

Hence by using {10} and {11},

$$\emptyset_A = (\Delta_A)\,(O_{total} - O_m) \qquad \textbf{\{12\}}$$

Hence, by taking the fluorescent readout (F) and the optical density readout (O) of the mixed sample and the single cultured B sample we can calculate the total fluorescence of the species A in the mixture.

Finally we deduce the total fluorescence per cell $= \frac{\emptyset_A}{(O_{total} - O_m)}$ **{13}**

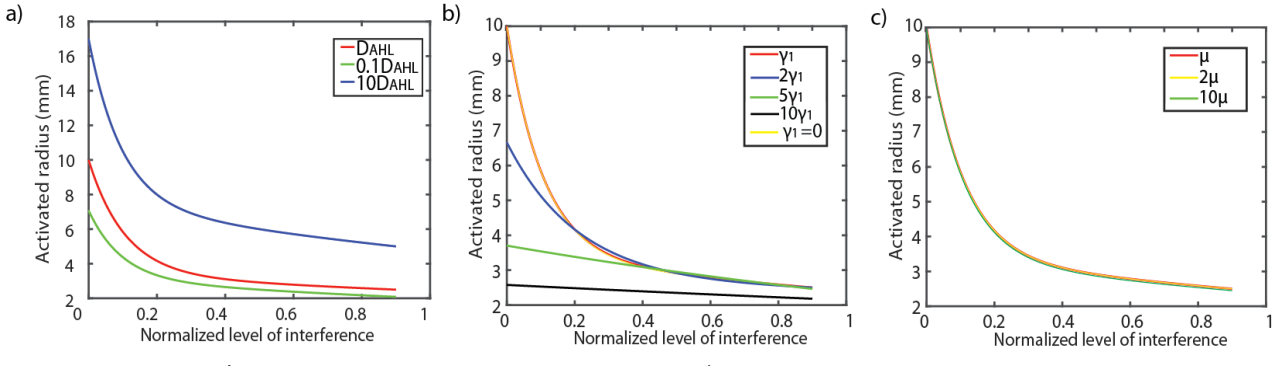

Figure S13: To understand the parameters that dictate the dynamics of the activation zone we changed (a) the sender AHL diffusion coefficient (b) the sender AHL degradation rate by the media (γ_1). In our experiment these values are constants. It can be seen that the degradation by the media is not a major contributor to the inhibition zone since even at zero degradation (γ_1 =0, yellow line), we see no deviations from γ_1 (red line). If the AHLs are degraded by the media at a higher rate, the activation radius for lower normalized interference values decreases, but above a certain γ_1 value, the radius for higher normalized interference seems to be affected as well. This is due to effect from γ_1 being comparable to the effect from the interferer. Additionally, we changed (c) the growth rate of the signal sender and observed no shift in the plot. This is due to the fact that the senders are already active when they are loaded into the plate such that levels of activation and degradation change proportionally.

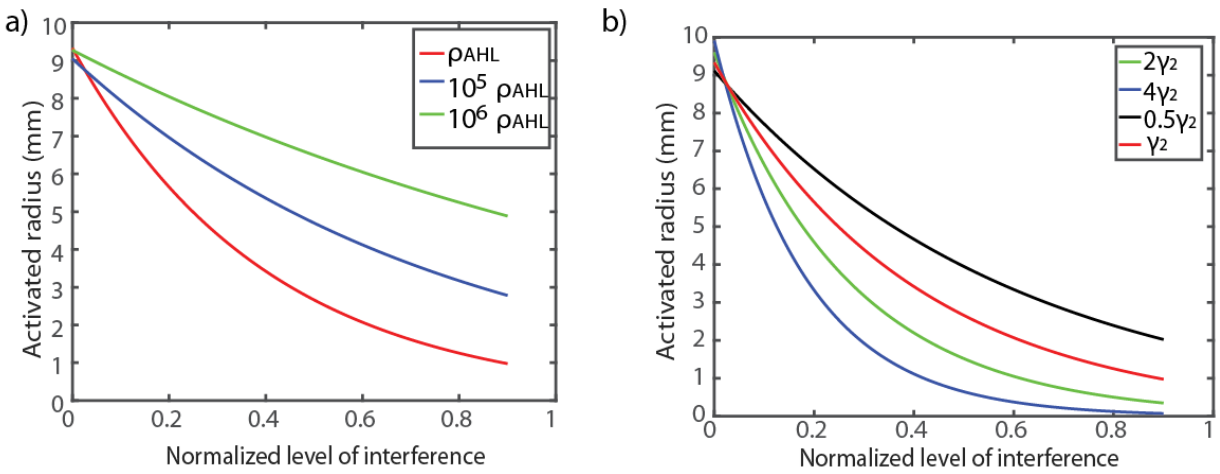

Figure S14: In simulations changing (a) the production rate of the AHL, (b) the degradation rate of the AHLs by the interferers. Compared to known quorum sensing production rates, the production rates used here are very large to have any significant effect on the plot. The plot is more sensitive towards the degradation rate of the interferers on the other hand, as seen in (b), doubling or halving the degradation rate shifts the plot significantly.

Testing the model for effects of the growth interactions, diffusion coefficients, degradation rates and internalization of the signal

To test the possible effect of growth influences on the sender-receiver system caused by the interferer we considered a competitive Lotka–Volterra equation (3),

$$\frac{\partial n}{\partial t} = \mu\, n\left(1 - \frac{n_{Total}}{s}\right) - \alpha_1\, n\, n_{interferer} \qquad \textbf{\{14\}}$$

where, α_1 is the growth effect the interfering species has on the sender-receiver system.

To test the effect of signal internalization we modified equation **{3}** such that,

$$\frac{\partial [AHL]}{\partial t} = D_{AHL}\nabla^2[AHL] + n_{AHL}\left(\rho_{AHL}\frac{[AHL]^{m_1}}{[AHL]^{m_1} + {\theta_1}^{m_1}} + \rho_{b1}\right) - \gamma_1[AHL] - \alpha_2\, n_{interferer}\frac{[AHL]^{m_4}}{[AHL]^{m_4} + {\theta_4}^{m_4}} \qquad \textbf{\{15\}}$$

where, α_2 is the AHL internalizing rate per interfering cell which is modulated by the number of AHLs present in the vicinity of the interferer.

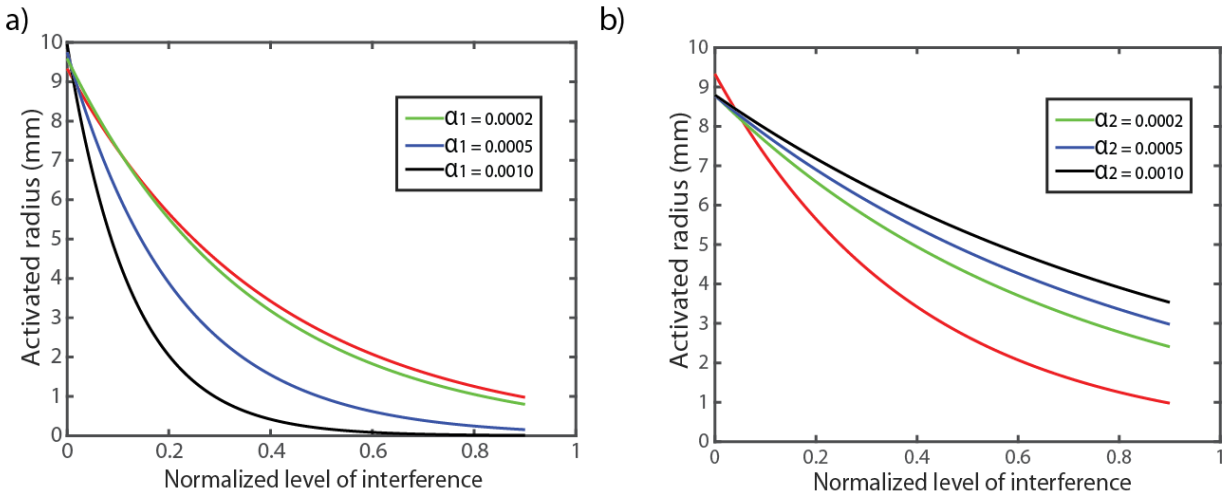

Figure S15: Change in activation dynamics as a result of growth interactions between species (a) or AHL internalization (b). To simulate these conditions, we used equations **{14} and {15}.** For both conditions, we assume that there is no AHL degradation by the interference strain, the influence of the interferer on the receiver is solely due to either growth influences or AHL internalization. The red curve represent the usual case when the interferer degrades the AHL, plotted here for comparison. For (b) we used, m_4 = 2.5 and $\theta_4 = 70\ nM$.

.

Supplemental References:

1. **Danino T**, **Mondragón-Palomino O**, **Tsimring L**, **Hasty J**. 2010. A synchronized quorum of genetic clocks. Nature **463**:326–330.

2. **Milo R**. 2013. What is the total number of protein molecules per cell volume? A call to rethink some published values. Bioessays **35**:1050–1055.

3. **Bomze IM**. 1995. Lotka-Volterra equation and replicator dynamics: new issues in classification. Biol Cybern **72**:447–453.